

Shining a Hot Light on Emerging Photoabsorber Materials: The Power of Rapid Radiative Heating in Developing Oxide Thin-film Photoelectrodes

Ronen Gottesman,^{a*} Isabella Peracchi,^{a,b} Jason L. Gerke,^{a,b} Rowshanak Irani,^a Fatwa F. Abdi,^a and
Roel van de Krol^{a,b*}

^aInstitute for Solar Fuels, Helmholtz-Zentrum Berlin für Materialien und Energie GmbH, Hahn-Meitner-Platz 1, 14109 Berlin, Germany.

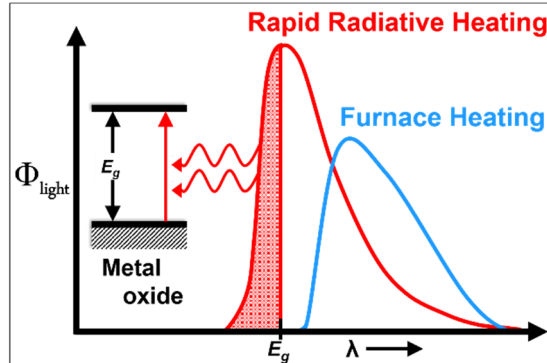
^bInstitut für Chemie, Technische Universität Berlin, Straße des 17. Juni 124, 10623 Berlin, Germany.

ronen.gottesman@helmholtz-berlin.de; roel.vandekrol@helmholtz-berlin.de

Abstract:

The unique possibilities of rapid thermal processing (RTP) for overcoming two significant challenges in the development of oxide thin-film photoelectrodes are demonstrated. The first is the need to exceed normal temperature limits for glass-based F:SnO₂ substrates (FTO, ~ 550 °C) to achieve the desired density, crystallinity, and low defect concentrations in metal oxides. Flash-heating of Ta₂O₅, TiO₂, and WO₃ photoelectrodes to 850 °C is possible without damaging the FTO. RTP heating-rate dependencies suggest that the emission spectrum of the RTP lamp, which blue-shifts with increasing heating power, can significantly influence the crystallization behavior of wide-bandgap photoelectrodes (≥ 1.8 eV). The second challenge is avoiding the formation of structural defects, trap states, grain boundaries, and phase impurities, which can be particularly difficult in multinary metal oxides. RTP treatment of α -SnWO₄, a promising photoanode material, resulted in an increase in grain size and favorable crystallographic re-orientation, culminating in a new performance record.

TOC



The most critical component in all solar energy conversion applications such as photoelectrochemical (PEC) water splitting, CO₂ reduction, and photovoltaics (PV) is the semiconducting photoabsorber.¹⁻³ Metal oxides are an important class of materials known for their chemical stability and wide-ranging and tunable multi-functionalities in numerous energy conversion applications. However, despite the many unique advantages they can offer as photoabsorber materials (wide range of bandgap energies, stability in aqueous solutions, low toxicity, and low-cost processing),⁴ metal oxide-based PEC water-splitting devices have shown only moderate efficiencies (< 8 %).⁵ Unlike conventional semiconductors such as silicon, many oxide semiconductors are limited by slow charge transport due to their ionic nature that leads to the formation of small polarons, causing carrier localization.^{6,7} Therefore, the successful development of practical solar water splitting applications is directly dependent on the emergence of new, more efficient oxides that also fulfill the criteria of stability, low toxicity, and low cost. Accomplishing this task requires the development and use of innovative approaches that accelerate materials discovery, such as computational predictions, together with high throughput experimentation and combinatorial methodologies.⁸⁻¹⁰

However, high throughput experimentation of metal oxides is often hampered by the need for a high-temperature crystallization step and the accompanying long processing times. Moreover, the loss of

volatile elements (e.g., Bi, Zn, Ge, Cd) during this sintering step can lead to poor compositional control for certain oxides.¹¹⁻¹⁴ These limitations can be detrimental to the quality of thin films that are only a few hundred nanometers thick and, therefore, to the optoelectronic properties and stability of the photoelectrodes.¹⁵ Furthermore, many metal oxides require growth/annealing temperatures up to 850 – 1000 °C or more in order to achieve the desired high density, high crystallinity, and low defect concentrations.^{12,16,17} Finally, the common use of glass-based transparent conductive substrates in PEC applications presents a technological challenge due to their softening above 350 – 550 °C (depending on the type of glass/conductive layer),^{18,19} preventing heating to the high temperatures that many metal oxides require. The standard, most commonly used transparent conductive substrate for PEC research and research on emerging PV materials (such as quantum-dots and halide perovskites) is a fluorine-doped tin oxide (FTO) film deposited on soda-lime glass, which can withstand temperatures up to 550 ± 50 °C for periods of several hours without softening or extensive loss of optical transmittance and electrical conductivity. FTO was, however, reported to remain stable after short heating times ($\approx 10^1 - 10^3$ sec) at 800 – 1000 °C,^{20,21} a temperature range which is well suited for processing many metal oxides (vide supra). A fast, uniform thermal processing method may thus offer a way to rapidly and briefly heat materials at the required temperatures without damaging their glass-based transparent conductive substrates and maintaining good optical transmittance and electrical conductivity.

One such possibility is using radiative heating, in contrast to convection/conduction heating methods by means of conventional furnaces. Rapid thermal processing (RTP) is a radiative heating method that was initially developed for the industrial fabrication of high-quality semiconductor devices and nanoelectronics applications.^{22,23} Its fast heating and cooling rates ($\sim 50 - 400$ °C/sec) enable only the desired physical or chemical processes, such as dopant activation, to be completed while preventing or suppressing unwanted processes. Most RTP systems use quartz halogen lamps for heating, but monochromatic light (e.g., lasers) has also been used in order to selectively heat semiconductor materials using photon energies above their band gaps.²⁴ RTP has not yet been used extensively for

the development of thin-film metal oxide photoelectrodes, primarily due to the relatively high cost of RTP systems as well as a possible misconception that it is mainly useful in industrial environments because it allows fast processing of large numbers of samples. Fortunately, the increasing number of more affordable, smaller RTP systems for R & D purposes in recent years should help accelerate the development of new photoabsorbers.

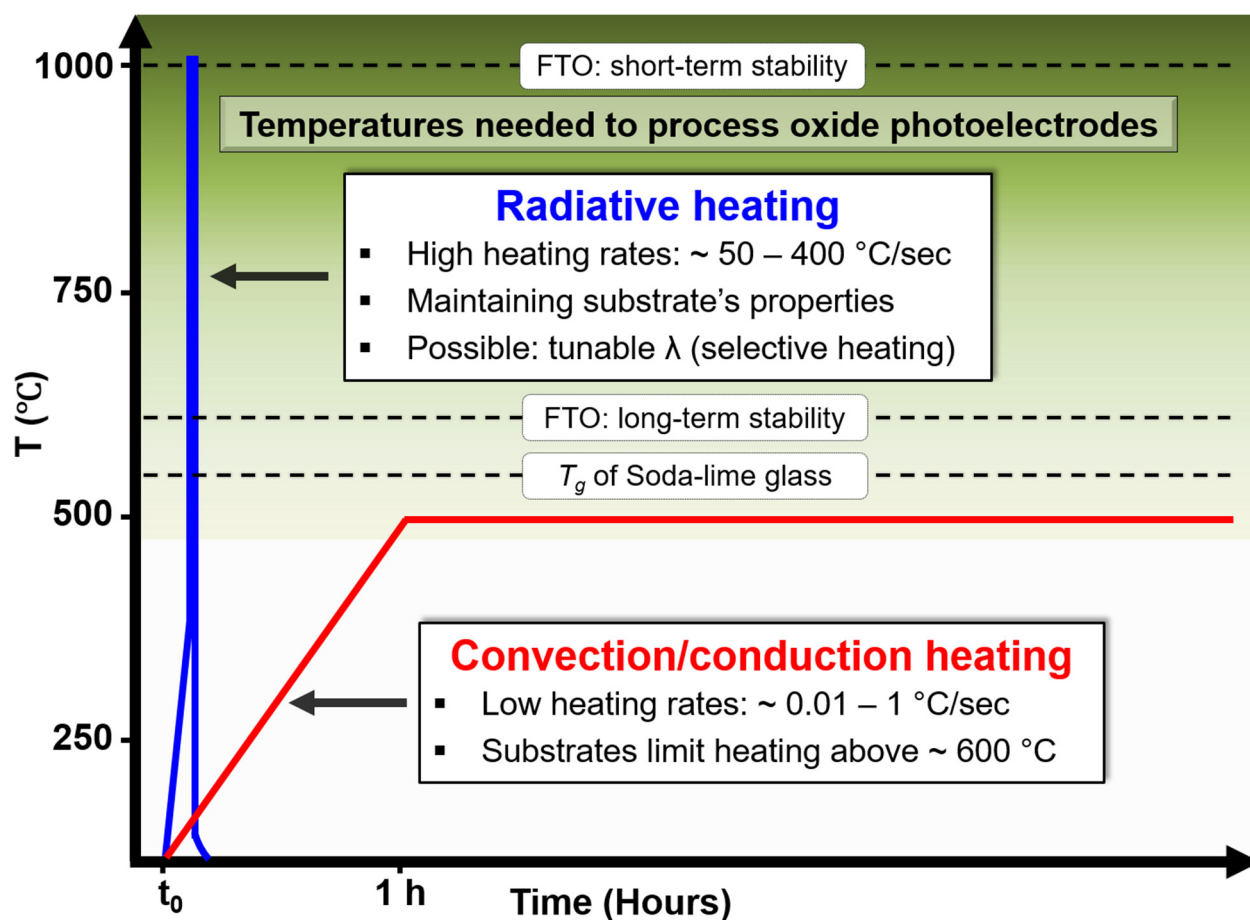


Figure 1. General characteristic temperature vs. time profiles of RTP (radiative heating) and conventional furnace heating (convection/conduction heating). The processing temperatures for oxide photoelectrodes and the thermal stability windows of typical soda-lime glass-based FTO substrates are shown. To avoid breaking the glass due to thermal shock when heating to high temperatures during RTP, photoelectrodes would typically require pre-heating below the substrates' glass transition temperatures (not shown).

Figure 1 illustrates the temperature vs. time profiles of RTP systems (radiative heating) and conventional furnaces (convection/conduction heating) together with the temperatures needed to process oxide photoelectrodes and the thermal stability windows of typical soda-lime glass-based FTO substrates. Recently, we have reported the use of RTP in overcoming synthesis and phase-purity challenges in the emerging photocathode material CuBi_2O_4 .^{15,25} We have shown a complete solid-state

reaction between 240 nm Bi₂O₃ and 300 nm CuO films at 650 °C within 10 minutes without damaging the glass-based FTO substrates and without degrading their properties. Conventional furnace heating of similar films for 72 h at 500 °C did not result in phase-pure CuBi₂O₄.²⁵ Furthermore, RTP was used to study the effect of different temperatures on films with thickness gradients, showing that 25 – 250 nm films that were rapidly processed at 650 °C were phase-pure, whereas ‘conventional’ furnace annealing at 400 – 500 °C resulted in the segregation of phase impurities.¹⁵ Many known and undoubtedly still-unknown metal oxides require processing temperatures even higher than 650 °C, calling for the broader usage of RTP in developing novel, more efficient metal-oxide photoelectrodes. In this work, we demonstrate the unique possibilities offered by RTP to overcome two significant challenges in the development of metal-oxide thin-film photoelectrodes.

The first challenge is the need to (briefly) exceed the normal temperature limit for glass-based FTO substrates (~ 550 °C) without thermally degrading their properties. The second challenge, discussed in the subsequent section of the manuscript, is to synthesize multinary metal oxides while avoiding the formation of structural defects, such as trap states, grain boundaries, and phase impurities. The presence of impurity phases that are randomly intermixed with the desired photoabsorber material can be particularly harmful to the photoelectrode performance and stability.¹⁵ We will show that RTP can overcome the first challenge with Ta₂O₅, TiO₂, and WO₃, all of which are extensively studied materials for PEC water splitting.^{26–35} The ability of RTP to address the second challenge will be demonstrated with the ternary α -SnWO₄,³⁶ which recently attracted attention as a potential candidate for solar water oxidation.^{37–41} For all these materials, we find that heating by RTP results in superior crystallinity, electronic properties, and performance when compared with conventional furnace heating.

Despite the extensive use of Ta₂O₅, TiO₂, and WO₃ for a wide range of solar energy conversion applications, these ceramic oxides have melting temperatures above 1500 °C (at 1 bar),¹² indicating that they require temperatures greater than 550 °C to provide sufficient kinetics for high density, better crystallinity, and low defect concentrations that are desired from high-quality semiconducting

photoabsorbers.¹⁵ Ta₂O₅ is a refractory compound whose direct deposition and crystallization may require temperatures of 700 °C or more,^{42,43} although crystalline thin films can also be obtained at lower temperatures when using, e.g., molecular precursors or an RF plasma-assisted process.^{26–28,44} In contrast, crystalline films of TiO₂ and WO₃ can be easily obtained at temperatures well below 550 °C for all common synthesis methods.

Ta₂O₅, TiO₂, and WO₃ films were deposited on FTO by pulsed laser deposition (PLD) and flash-heated by RTP to 850 °C and compared with similar films heated by a conventional furnace at 500 °C (full experimental conditions are detailed in the supporting information). Figure 2a shows the X-ray diffractograms (XRD) of tantalum oxide (Ta_xO_y) films on FTO glass substrates, as-deposited at 10⁻⁶ mbar, after furnace heating (FH) for 72 h at 500 °C in air, and after RTP at 850 °C in O₂ and N₂ at a rate of ~90 °C/sec. Despite deposition at a substrate temperature of 500 °C, the as-deposited Ta_xO_y film is amorphous and appears black, suggesting the presence of oxygen vacancies as a result of deposition under low-pressure conditions. The FH-treated film became optically transparent but nonetheless remained amorphous. Remarkably, the RTP-treated films crystallized in about ≈ 5 sec (from 400 to 850 °C at 90 °C/sec). Heating under O₂ resulted in a crystalline Ta₂O₅ phase, as can be seen from the comparison with the Ta₂O₅ reference pattern. The XRD patterns of RTP-treated films under N₂ and Ar were almost identical, as seen in Figure S1. Therefore, we label the diffractogram of RTP under N₂ as RTP (N₂/Ar). Both films shared only several diffraction peaks with the reference pattern of Ta₂O₅ and had an increased absorption in the visible range, seen in Figure S2. Because the Ta-O system is known to uphold multiple and very similar metastable phases,⁴⁵ the exact structural determination of the RTP-treated Ta_xO_y films under N₂ or Ar cannot be reliably determined from this set of data and is beyond the scope of this work. The oxidation states of Ta and O at the surfaces of the photoelectrodes were studied by X-ray photoelectron spectroscopy (XPS), shown in Figure S3. As expected, heating in an oxygen atmosphere resulted in the formation of a Ta₂O₅ film, confirmed by binding energies that contribute to Ta⁵⁺ and lattice oxygen O²⁻.^{28,46–48} However, films heated in the

presence of N₂ and Ar showed a mixture of several Ta oxidation states lower than the typical +5 state. The lower binding energies for the Ta 4f states indicate a lower average oxidation state, implying a lower O:Ta ratio in the films, which is expected when annealing the films in an oxygen-poor atmosphere. We note that nitrogen was not detected in films heated under N₂, ruling out the possibility of nitrogen incorporation.

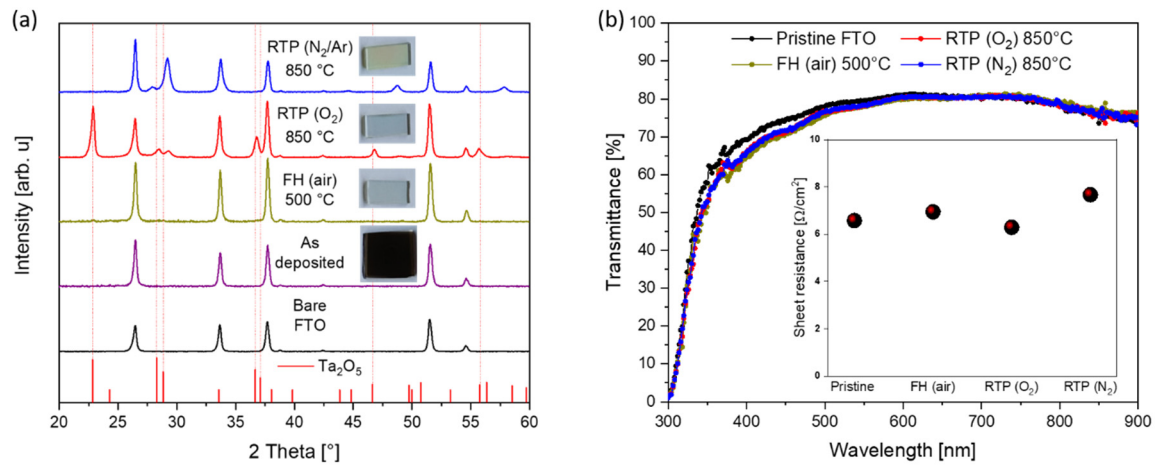


Figure 2. a) X-ray diffractograms of a bare FTO substrate and 50 nm Ta_xO_y films deposited on FTO: as-deposited, after FH for 72 h at 500 °C in air, and after RTP at 850 °C in O₂ and N₂ at a rate of ~ 90 °C/sec. Ta₂O₅ PDF: 01-082-9637. b) Transmittance and sheet resistance (inset) of the corresponding substrates.

To confirm that the RTP treatment does not degrade the properties of the glass and the FTO, the transmittance and sheet resistance (T and R_s , respectively) of bare FTO substrates were measured after flash-heating by RTP at 850 °C in different gas atmospheres. Figure 2b shows that the T and R_s of substrates heated by RTP (at 90 °C/sec) were similar to those heated in a regular furnace at 500 °C, demonstrating that RTP can successfully overcome the first challenge and exceed the normal temperature limit for glass-based FTO substrates (~ 550 °C) without thermally degrading their properties. Furthermore, rapid heating of thicker photoelectrodes (~ 200 – 700 nm) at 800 – 1000 °C without degrading the FTO substrates has been shown to successfully yield high crystallinity, demonstrated with TiO₂,⁴⁹ Fe₂O₃,¹⁷ and CuFe₂O₄²¹ for solar water splitting as well as perovskite solar cells.²⁰

Surprisingly, the heating rates of RTP had a pronounced effect on the degree of crystallization of the Ta_xO_y films, which is different than what one might intuitively expect from such short heating times. Figure 3a shows that the crystallinity of Ta_2O_5 increases with higher heating rates, visibly observed by the films' increased homogeneity and demonstrated by the growth of the peaks at 22.83° , 28.24° , 28.85° , and 36.67° (circled by the dashed lines). This may seem counterintuitive from the perspective of conventional FH because, at higher heating rates, the samples are given less time to crystallize. The difference in heating rates caused a 15°C temperature overshoot, which took 3 seconds longer to dissipate below 850°C . This difference is arguably too minor to be the sole cause of the increased effective heating. As a result, we looked into the effect of heating rates on the emission spectra of the RTP lamps (tungsten halogen in our RTP system) as a possible additional reason for increased effective heating.

A significant difference between the heating methods is that in RTP, the temperature of the lamps significantly influences the spectral distribution of the radiant flux. According to Planck's black-body radiation law,⁵⁰ as the temperature of the lamps increases, the spectral radiant flux (SRF) increases, and the maximum of the SRF spectrum shifts to shorter wavelengths, as shown by the calculated black-body radiation curves in Figure 3b.⁵¹ We note that spectral radiative flux measurements were not possible in our RTP system. However, Figure S4 displays measured spectral irradiances at different powers/temperatures of a 1000 W tungsten halogen lamp,⁵² showing spectral fluxes similar to the calculated fluxes as in Figure 3b. The spectral shift to shorter wavelengths is often ignored in RTP heating because it is less relevant for, e.g., silicon processing; due to its small bandgap of 1.1 eV, Si absorbs most photons emitted by the tungsten halogen lamp, regardless of the lamp's color temperature. However, illumination at color temperatures above $\approx 3000^\circ\text{C}$ can be potentially significant for photoelectrodes with bandgaps that extend into the visible range, as shown by the dashed vertical line at 1.8 eV. For Ta_2O_5 , which has a bandgap energy of ≈ 3.9 eV ($\lambda \approx 315$ nm), it is mainly the higher-energy photons that contribute to the efficient heating of the material (Figure 3b). Higher

heating rates are obtained by delivering more power to the tungsten-halogen lamps; this shifts the maximum of the SRF spectrum to higher energies (shorter wavelengths) and results in more effective heating of the Ta₂O₅ film. Finally, more research with higher temporal resolutions is required to detect instantaneous (< 0.1 sec, the temporal resolution of our RTP system) higher surface temperatures and their decays, which will improve understanding of the relationship between higher absorption (due to higher radiative heating rates) and better heating efficiency of wide bandgap semiconductors.

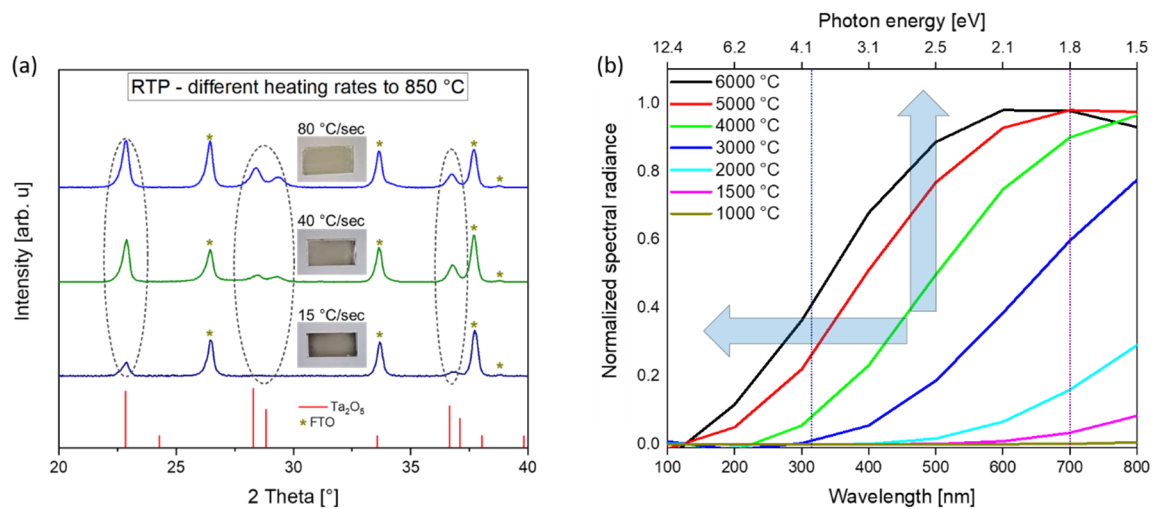


Figure 3. a) X-ray diffractograms of Ta_xO_y films deposited on FTO after different RTP heating rates under O₂ at 850 °C: 15, 40, and 80 °C/sec. Ta₂O₅ PDF: 01-082-9637. b) Black body spectral radiance as a function of color temperature calculated from data in ref⁵¹. At higher temperatures, the radiant flux increases, and its maximum shifts to shorter wavelengths. The dashed vertical lines represent the bandgap energies of pristine Ta₂O₅ and a typical small-bandgap metal oxide photoabsorber that absorbs most of the visible light (≈ 3.9 eV/ 315 nm, 1.8 eV/ ~ 700 nm, respectively).

To demonstrate the advantages of flash-heating at higher temperatures on a broader range of established metal oxide photoelectrodes with narrower bandgap energies, RTP was used to heat 30 nm TiO₂ and WO₃ photoelectrodes at 850 °C as well. After deposition by PLD, each photoelectrode was divided along its centerline, allowing for different heating treatments (RTP vs. FH) of two essentially identical samples. To focus only on the effect of the temperature profile, the gas atmosphere during RTP was kept as an 80:20 mixture of N₂:O₂, the same as the ambient air that was used in FH. For both materials, the RTP and FH treatments do not result in any differences in crystal structure and optical absorption, seen in Figure S5. We note that crystalline TiO₂ peaks were not observed at all, which we attribute to the minimal film thickness of ~ 30 nm and the overlap of these peaks with the FTO substrate. Therefore, any conclusion about the influence of RTP vs. FH on the crystallinity of TiO₂ is

not possible in this case. However, both RTP-treated TiO₂ and WO₃ photoelectrodes exhibited slightly higher photocurrents than their FH-treated counterparts did over the entire potential range, seen in Figure 4a. We note that in the case of WO₃, the synthesis requires further optimization for the reason that a broad oxidation peak was visible at lower potentials, indicating the presence of reduced W⁵⁺.^{53,54} The photocurrent onset potential of the RTP-treated WO₃ was significantly more negative than that of the FH-treated WO₃ (0.55 V vs. 0.85 V vs. RHE). These results show that the improvements of the RTP-treated photoelectrodes are not due to significant changes in the crystal structure or optical absorption but to more subtle changes in the electronic structure that are related to, for example, the nature and number of trap states in the material.

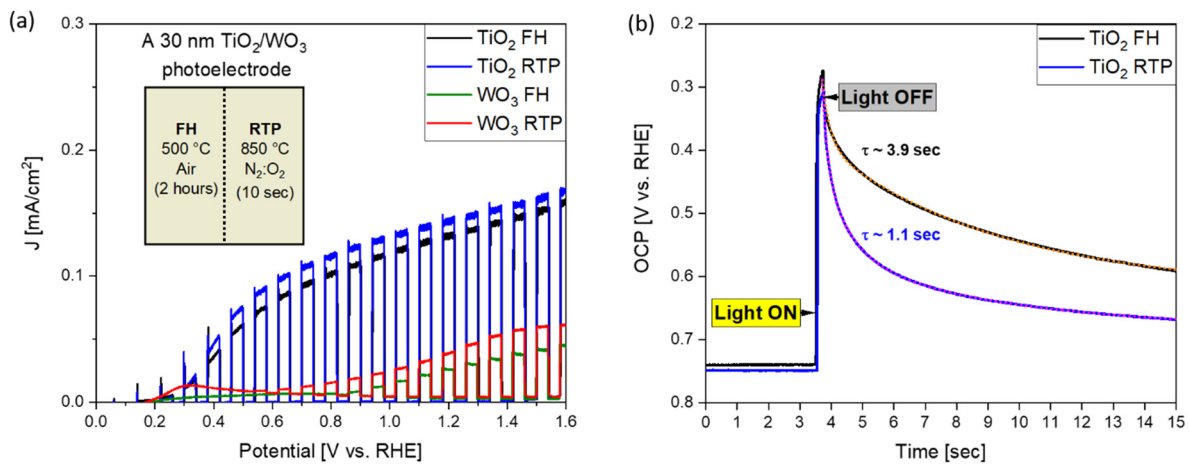


Figure 4. a) Chopped linear sweep voltammetry scans of 30 nm TiO₂ and WO₃ photoelectrodes divided along their centerline allowing for different heating treatments: FH for 2 hours at 500 °C (air) or flash-heating to 850 °C (N₂:O₂, 80:20 % 15 °C/sec. b) Open circuit potential decay of the RTP- and FH treated TiO₂ photoelectrodes after a short light-perturbation of 0.2 seconds. Performed in 0.1 M boric acid (pH 9), front-side illumination is presented.

To evaluate the differences in electronic structure between the RTP- and FH-treated photoelectrodes, transient open circuit potential (OCP) decay measurements were performed.⁵⁵⁵⁶ When the electrode is illuminated under open-circuit conditions, the concentration of minority carriers increases and the quasi-Fermi levels for electrons and holes split to produce a photovoltage. The band bending in the material decreases, which means that the bulk Fermi level rises (in an n-type semiconductor) and the OCP becomes more negative. When the light is turned off, electrons and holes begin to recombine,

and the OCP decays to the initial dark value. Provided that the photoelectrodes are stable, measured under the same conditions, and their Fermi level positions in the dark are similar (similar OCPs), the kinetics of recombination can be qualitatively compared. Figure 4b displays the OCP decays for TiO₂ photoelectrodes annealed with FH and RTP after illuminating the sample for 0.2 seconds with AM1.5G light (100 mW/cm²). Upon turning off the light, the OCP takes several seconds to decay to its dark value. This relatively slow decay indicates that the recombination occurs via trap states in the material. The exponential decay rate of the RTP-treated TiO₂ was ~ 4 times faster than the decay rate of its FH-treated counterpart. The faster decay is attributed to a lower number of surface trap states in the RTP-treated TiO₂, which means that more carriers recombine via (faster) band-to-band recombination that is present in both RTP- and FH-treated films. The lower number of trap states explains the higher photocurrents, although the relatively modest improvement suggests that the photocurrent of these 30 nm films is mainly limited by light harvesting, with carrier trapping playing only a minor role.

We briefly note that, as expected, pristine Ta₂O₅ does not show any PEC activity due to poor light-harvesting based on its large bandgap energy. In contrast, both RTP-treated Ta_xO_y under N₂ or Ar photoelectrodes display APCE onsets at ~ 450 nm and photocurrents in the range of ~ 20 – 25 μA/cm² (at 1.23 V vs. RHE), as shown in Figure S6. The APCE onset shift to ~ 450 nm can be attributed to sub-bandgap absorption by defects associated with e.g. oxygen vacancies, followed by charge injection into the electrolyte from these states.

Now, we turn our attention to the ternary photoabsorber α-SnWO₄, a promising photoanode that typically requires heating under an inert atmosphere to mitigate the oxidation of Sn²⁺ to Sn⁴⁺. Moreover, the annealing temperature needs to be kept below 550 °C to prevent undesired phase changes; in a recent study where only conventional FH was used,³⁸ we have shown that heating at temperatures between 600 and 700 °C, a Sn_{0.23}WO₃ impurity phase forms in α-SnWO₄ films deposited on quartz substrates. Further temperature increase to 750 °C resulted in a phase transformation to β-SnWO₄, the high-temperature polymorph of α-SnWO₄, while the amount of Sn_{0.23}WO₃ decreased.

Furthermore, the electronic structure of α -SnWO₄ was shown to be highly dependent on heating times and temperature in both experimental and computational studies,^{37–39,57} which further emphasizes the need for a better-controlled and tunable technique to anneal α -SnWO₄. Here, 100 nm amorphous SnWO₄ films deposited on FTO with PLD were heated under argon at 550 °C by either RTP or FH. The RTP-treated films were heated for 1 – 8 minutes and compared with identical films heated by FH for 2 hours, which was previously reported as the optimized heating time.^{38,39} Heating by both methods resulted in single-phase α -SnWO₄ comprised of elongated grains, seen in Figures S7, S8. However, all RTP-treated photoelectrodes showed higher crystallinity than the FH-treated photoelectrode, as seen by the narrower FWHMs of the (040) and (121) peaks in Figure S9.

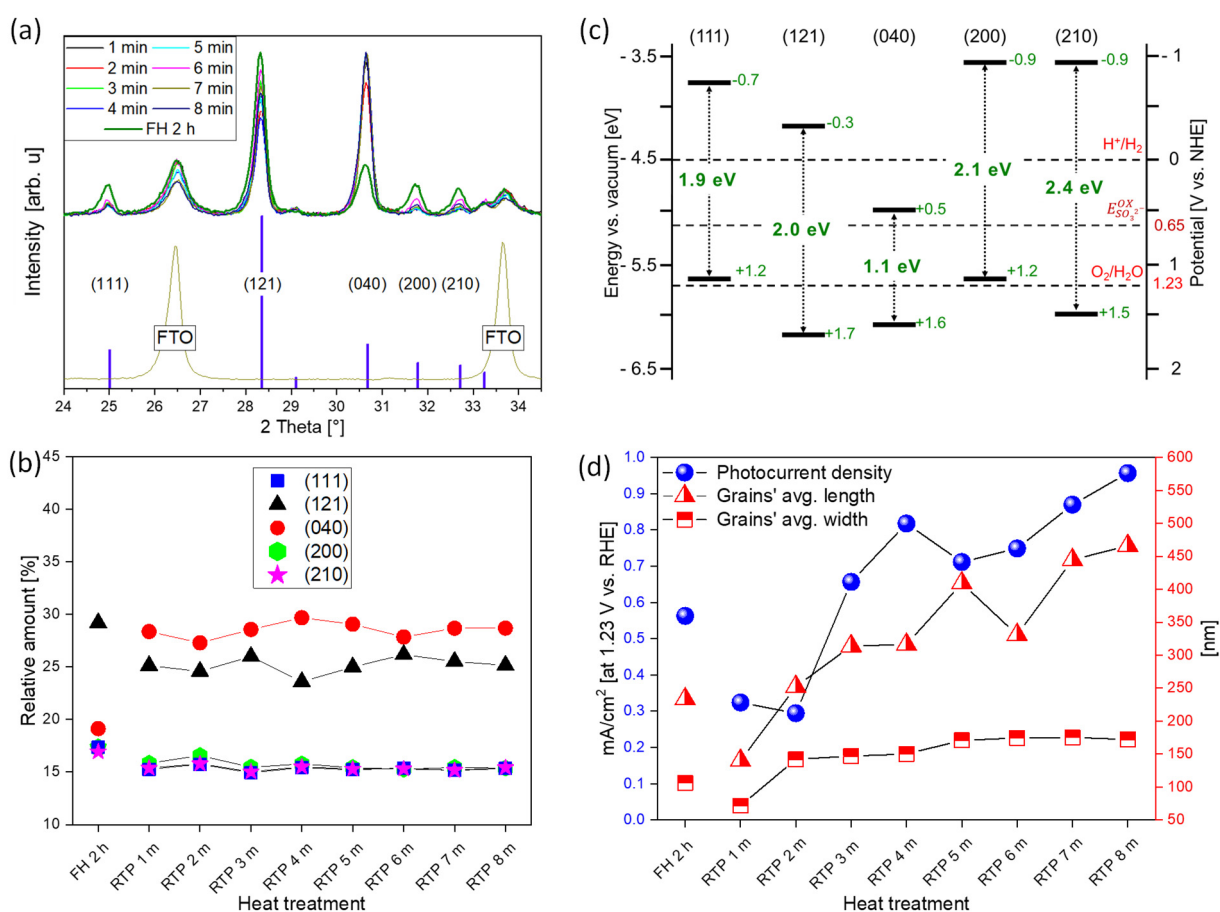


Figure 5. a) X-ray diffractograms showing the 24° – 34.5° range of the 1 – 8 min RTP-treated and FH 2 h-treated 100 nm α -SnWO₄ photoelectrodes, plotted on the same baseline, with bare FTO as a reference. The diffraction peaks of the (111), (121), (040), (200), and (210) predominant Miller indices are labeled. b) Relative amount of the predominant Miller indices in all films. c) Band energy levels of the (111), (121), (040), (200), and (210) – oriented α -SnWO₄, constructed from data in references.^{40,41} d) Photocurrent values (dark currents are subtracted) for sulfite oxidation at 1.23 V vs. RHE of the α -SnWO₄/NiO_x photoelectrodes and the average grain sizes of the particles plotted against the type and duration of heating treatment.

Additionally, careful examination of the XRD data shows that the RTP and FH treatments affect the crystallographic orientations differently in the α -SnWO₄ polycrystalline films. Figure 5a displays the normalized diffractograms of both RTP- and FH-treated photoelectrodes in the 2θ range of 24° – 34.5°, which contains the (111), (121), (040), (200), and (210) Miller indices of α -SnWO₄. Recently, Harb et al. reported DFT calculations that show anisotropic characteristics of predominantly exposed facets (low-Miller index surfaces) of α -SnWO₄ and their effect on the photocatalytic performance for H₂ and O₂ evolution reactions.^{40,41} To enable the evaluation of the subsequent effect of the different crystallographic orientations and distribution of exposed facets on the films' properties, the intensity value of each Miller index in Figure 5a was divided by the sum of all intensities and labeled as the “relative amount” of that Miller index. Figure 5b shows the partial amounts of the (111), (121), (040), (200), and (210) in all films, plotted against the type and duration of the heating treatment. Two similarities are observed in both heating methods: i) the (121) facet is predominant, with an average partial amount of 25.1 % in the RTP-treated films and 29.2 % in the FH-treated film, and ii) the (111), (200), and (210) facets have, on average, similar partial amounts of ~ 15 – 17 %. However, a clear difference between the two methods is the relative amount of the (040) facet. In the FH-treated film, the partial amount of (040) facet is 19.1 %, whereas, in the RTP-treated films, its average partial amount was ~ 28.8 %, showing, therefore, the RTP-treated films contain crystals that are primarily (040) oriented.

Figure 5c shows the band energy levels of the (111), (121), (040), (200), and (210) – oriented α -SnWO₄ that were reconstructed from the reports of Harb et al.^{40,41} The bandgap energy of the (040)-oriented material is 1.1 eV, substantially narrower than the 1.9 – 2.4 eV bandgap energies of the (111), (121), (200), and (210) orientations. Therefore, the optical properties of films heated by the different methods are expected to be different. Figure S10 displays the absorption, reflection, and transmittance of all films. The absorption of the RTP-treated films indeed seems to be higher by 3 – 5 %. However, that is not sufficient to conclude that it is a direct result of an increased partial amount of the 1.1 eV (040)

orientation. Moreover, differences in the reflection and transmittance due to the different morphology and crystallographic orientation are very plausible. Further studies are required to elucidate the mechanisms of different crystallographic orientations in the RTP- and FH-treated films. However, we hypothesize that the significant differences in heating rates are a major contributing factor, as recently reported by us with CuBi_2O_4 films.²⁵ In RTP-treated films, the high heating rate (10 K/sec) brings the system into a steady-state temperature of 550 °C in ≈ 1 min. However, in FH-treated films, a slower heating rate (10 K/min) brings the system into a steady-state temperature of 550 °C after ≈ 1 h. In each case, it is expected that the diffusion processes and atomic rearrangement would not be identical, resulting in different orientations and grain sizes (vide infra).

Figure 5d presents the photocurrent values for sulfite oxidation at 1.23 V vs. RHE, as well as the average grain sizes plotted against the type and duration of the heating treatment of $\alpha\text{-SnWO}_4$ photoelectrodes. The linear sweep voltammetry scans of all films are shown in Figure S11. All films were coated with a 20 nm NiOx protection layer prior to PEC measurements.^{37,39} The FH-treated photoelectrode displays a photocurrent of 0.57 mA/cm², whereas the 1 and 2 min RTP-treated photoelectrodes exhibited much lower photocurrents. However, for photoelectrodes that are RTP-treated from 3 to 8 min, the photocurrents are increased from ~ 0.65 mA/cm² to ~ 0.95 mA/cm², which is higher than the previously reported benchmark value of ~ 0.75 mA/cm².³⁷ The low photocurrents of the 1 and 2 min RTP-treated photoelectrodes are likely a result of smaller grains which were reported to affect the photoconductivity of $\alpha\text{-SnWO}_4$,³⁸ and insufficient heating times that subtly affected their defect concentration. The higher photocurrents of the 3 – 8 min RTP-treated photoelectrodes can be attributed to one or more of the following factors: i) higher crystallinity, as indeed evidenced by the narrower FWHMs of the XRD peaks, ii) subtle changes in the electronic structure (e.g., defects, surface trap states), as shown above for the case of TiO_2 , iii) larger grains (primarily in length), iv) minor increase in absorption due to dominant (040) orientation, or v) more positive valence bands for the (121) and (040) orientations; these are in fact > 1 V more positive than the oxidation potential of sulfite,

which increases the driving force for charge transfer. Whereas factors i – iii are highly likely to contribute to the higher photocurrents, conclusive proof and accurate quantification of increased light harvesting for the (040) orientation and more efficient charge transfer processes for the (040) and (121) orientations requires further elaborate studies e.g., on singly oriented or epitaxial films.

In summary, the unique possibilities and impact of RTP for overcoming two significant challenges in the development of oxide thin-film photoelectrodes were shown. The first challenge is the need to exceed the normal temperature limit (~ 550 °C) for the most commonly used glass-based FTO substrates for PEC and PV research without thermally degrading its properties. This was successfully demonstrated by flash-heating Ta₂O₅, TiO₂, and WO₃ photoelectrodes to 850 °C without damaging the FTO. The second challenge is to avoid structural defects and undesired phase transformations, which may potentially be harmful to the photoelectrode performance and stability. While we have previously shown that RTP can reduce the formation of impurity phases for other materials, like CuBi₂O₄,^{15,25} clear evidence for this effect is not present in our α -SnWO₄ data. Nevertheless, we showed that RTP reduced the number of trap states in TiO₂ and resulted in superior crystallinity, electronic properties, and performance of α -SnWO₄ when compared with conventional furnace heating of similar photoelectrodes, culminating in a new performance record for α -SnWO₄ for sulfite oxidation. The improvements are not due to significant structural or optical changes but to more subtle changes in the electronic structure that are likely related to the nature and number of trap states in the material and crystallographic orientation. We also found that a higher heating rate improves the crystallization of Ta₂O₅, even though high heating rates imply shorter exposure times to elevated temperatures. We attribute this to the increase in lamp power that is needed to sustain the higher heating rate, which shifts the maximum of the spectral radiant flux (SRF) of the lamp to shorter wavelengths. This results in an overlap of the SRF spectrum with the absorption spectrum of the material, which allows efficient heating of the material by direct absorption of the emitted photons. These findings offer valuable

insights for the further optimization of RTP systems and heating protocols and offer a promising path towards the development of efficient complex oxide-based photoelectrodes on glass-based substrates.

Acknowledgment

The authors would like to acknowledge Marco Favaro for fruitful discussions, Rene Gunder for XRD user support, and Christian Höhn and Karsten Harbauer for technical support. The authors also thank Stefan Würfl for his experimental assistance.

Associated Content: The Supporting Information is available free of charge at:

Full experimental details: materials, film deposition parameters, furnace heating, and rapid thermal processing protocols, X-ray diffraction (XRD), X-ray photoelectron spectroscopy (XPS), UV-VIS measurements, photoelectrochemical measurements; supporting figures: XRD of Ta_xO_y photoelectrodes after RTP at 850 °C in Ar and N_2 , absorption of RTP-treated Ta_xO_y photoelectrodes under O_2 , Ar and N_2 , XPS spectra of Ta 4f, and O 1s core levels, measured spectral irradiances of a tungsten halogen lamp at different powers/temperatures, XRD of TiO_2 , WO_3 photoelectrodes heated by RTP and FH, photoelectrochemical measurements of RTP-treated Ta_xO_y photoelectrodes under O_2 , Ar and N_2 , XRD of α - $SnWO_4$ photoelectrodes heated by RTP and FH, UV-VIS measurements of α - $SnWO_4$ heated by RTP and FH, and LSVs of α - $SnWO_4$ heated by RTP and FH.

References

- (1) Bolton, J. R. Solar Fuels. *Science* (80-.). **1978**, *202* (4369), 705–712.
- (2) Sivula, K. Metal Oxide Photoelectrodes for Solar Fuel Production, Surface Traps, and Catalysis. *J. Phys. Chem. Lett.* **2013**, *4* (10), 1624–1633.
- (3) Lee, D. K.; Lee, D.; Lumley, M. A.; Choi, K. S. Progress on Ternary Oxide-Based Photoanodes for Use in Photoelectrochemical Cells for Solar Water Splitting. *Chem. Soc. Rev.* **2019**, *48* (7), 2126–2157.
- (4) Abdi, F. F.; Berglund, S. P. Recent Developments in Complex Metal Oxide Photoelectrodes. *J. Phys. D: Appl. Phys.* **2017**, *50*, 193002.
- (5) Chen, Y.; Feng, X.; Liu, Y.; Guan, X.; Burda, C.; Guo, L. Metal Oxide-Based Tandem Cells for Self-Biased Photoelectrochemical Water Splitting Metal Oxide-Based Tandem Cells for

- Self-Biased Photoelectrochemical Water Splitting. *ACS Energy Lett.* **2020**, *5*, 844–866.
- (6) Rettie, A. J. E.; Chemelewski, W. D.; Emin, D.; Mullins, C. B. Unravelling Small-Polaron Transport in Metal Oxide Photoelectrodes. *J. Phys. Chem. Lett.* **2016**, *7* (3), 471–479.
 - (7) Franchini, C.; Reticcioli, M.; Setvin, M.; Diebold, U. Polarons in Materials. *Nat. Rev. Mater.* **2021**, *6*, 560–586.
 - (8) Wang, C.; Ping, W.; Bai, Q.; Cui, H.; Hensleigh, R.; Wang, R.; Brozena, A. H.; Xu, Z.; Dai, J.; Pei, Y.; et al. A General Method to Synthesize and Sinter Bulk Ceramics in Seconds. *Science (80-.)*. **2020**, *368* (6490), 521–526.
 - (9) van de Krol, R.; Parkinson, B. A. Perspectives on the Photoelectrochemical Storage of Solar Energy. *MRS Energy Sustain. A Rev. J.* **2017**, *4*, E13.
 - (10) van de Krol, R. A Faster Path to Solar Water Splitting. *Matter* **2020**, *3* (5), 1389–1391.
 - (11) Sossi, P. A.; Fegley, B. Thermodynamics of Element Volatility and Its Application to Planetary Processes. *Rev. Mineral. Geochemistry* **2018**, *84* (1), 393–459.
 - (12) Brewer, L. The Thermodynamic Properties of the Oxides and Their Vaporization Processes. *Chem. Rev.* **1953**, *52* (1), 1–75.
 - (13) Lamers, M.; Fiechter, S.; Friedrich, D.; Abdi, F. F.; Krol, R. van de. Formation and Suppression of Defects during Heat Treatment of BiVO₄ Photoanodes for Solar Water Splitting. *J. Mater. Chem. A* **2018**, *6*, 18694–18700.
 - (14) Zurbuchen, M. A.; Lettieri, J.; Fulk, S. J.; Jia, Y.; Carim, A. H.; Schlom, D. G. Bismuth Volatility Effects on the Perfection of SrBi₂Nb₂O₉ and SrBi₂Ta₂O₉ Films. *Appl. Phys. Lett.* **2003**, *82* (26), 4711–4713.
 - (15) Gottesman, R.; Levine, I.; Schleuning, M.; Irani, R.; Abou-ras, D.; Dittrich, T.; Friedrich, D.; van de Krol, R. Overcoming Phase-Purity Challenges in Complex Metal Oxide Photoelectrodes: A Case Study of CuBi₂O₄. *Adv. Energy Mater.* **2021**, *11*, 2003474.
 - (16) MacManus-Driscoll, J. L.; Wells, M. P.; Yun, C.; Lee, J.-W.; Eom, C.-B.; Schlom, D. G. New Approaches for Achieving More Perfect Transition Metal Oxide Thin Films. *APL Mater.* **2020**, *8*, 040904.
 - (17) Wickman, B.; Bastos Fanta, A.; Burrows, A.; Hellman, A.; Wagner, J. B.; Iandolo, B. Iron Oxide Films Prepared by Rapid Thermal Processing for Solar Energy Conversion. *Sci. Rep.* **2017**, *7*, 1–9.
 - (18) Shen, J.; Green, D. J.; Tressler, R. E.; Shelleman, D. L. Stress Relaxation of a Soda Lime Silicate Glass below the Glass Transition Temperature. *J. Non. Cryst. Solids* **2003**, *324* (3), 277–288.
 - (19) Kawashima, T.; Ezure, T.; Okada, K.; Matsui, H.; Goto, K.; Tanabe, N. FTO/ITO Double-Layered Transparent Conductive Oxide for Dye-Sensitized Solar Cells. *J. Photochem. Photobiol. A Chem.* **2004**, *164* (1–3), 199–202.
 - (20) Sánchez, S.; Vallés-Pelarda, M.; Alberola-Borràs, J. A.; Vidal, R.; Jerónimo-Rendón, J. J.; Saliba, M.; Boix, P. P.; Mora-Seró, I. Flash Infrared Annealing as a Cost-Effective and Low Environmental Impact Processing Method for Planar Perovskite Solar Cells. *Mater. Today* **2019**, *31*, 39–46.
 - (21) Park, S.; Baek, J. H.; Zhang, L.; Lee, J. M.; Stone, K. H.; Cho, I. S.; Guo, J.; Jung, H. S.;

Zheng, X. Rapid Flame-Annealed CuFe₂O₄ as Efficient Photocathode for Photoelectrochemical Hydrogen Production. *ACS Sustain. Chem. Eng.* **2019**, *7* (6), 5867–5874.

- (22) Singh, R. Rapid Isothermal Processing. *J. Appl. Phys.* **1988**, *63*, R59–R114.
- (23) Fiory, A. T. Rapid Thermal Processing for Silicon Nanoelectronics Applications. *J. Miner. Met. Mater. Soc.* **2005**, *57* (6), 21–26.
- (24) Rebohle, L.; Prucnal, S.; Skorupa, W. A Review of Thermal Processing in the Subsecond Range: Semiconductors and Beyond. *Semicond. Sci. Technol.* **2016**, *31*, 103001.
- (25) Gottesman, R.; Song, A.; Levine, I.; Krause, M.; Islam, A. T. . N.; Abou-Ras, D.; Dittrich, T.; van de Krol, R.; Chemseddine, A. Pure CuBi₂O₄ Photoelectrodes with Increased Stability by Rapid Thermal Processing of Bi₂O₃/CuO Grown by Pulsed Laser Deposition. *Adv. Funct. Mater.* **2020**, *28*, 1910832.
- (26) Sarker, J. C.; Vasan, R.; Makableh, Y. F.; Lee, S.; Nusir, A. I.; Manasreh, M. O. Enhanced Performance of Surface Modified InAs Quantum Dots Solar Cell by a Sol-Gel Grown Tantalum Pentoxide Antireflection Coating. *Sol. Energy Mater. Sol. Cells* **2014**, *127*, 58–62.
- (27) Forster, M.; Potter, R. J.; Yang, Y.; Li, Y.; Cowan, A. J. Stable Ta₂O₅ Overlayers on Hematite for Enhanced Photoelectrochemical Water Splitting Efficiencies. *ChemPhotoChem* **2018**, *2* (3), 183–189.
- (28) Yu, X.; Li, W.; Li, Z.; Liu, J.; Hu, P. Defect Engineered Ta₂O₅ Nanorod: One-Pot Synthesis, Visible-Light Driven Hydrogen Generation and Mechanism. *Appl. Catal. B Environ.* **2017**, *217*, 48–56.
- (29) Kohlsdorf, A.; Taffa, D. H.; Wark, M. Microwave Assisted Synthesis of Ta₂O₅ Nanostructures for Photocatalytic Hydrogen Production. *J. Photochem. Photobiol. A Chem.* **2018**, *366*, 41–47.
- (30) Fujishima, A.; Honda, K. Electrochemical Photolysis of Water at a Semiconductor Electrode. *Nature* **1972**, *238*, 37–38.
- (31) Gottesman, R.; Tirosh, S.; Barad, H.-N.; Zaban, A. Direct Imaging of the Recombination / Reduction Sites in Porous TiO₂ Electrodes. *J. Phys. Chem. Lett.* **2013**, *4*, 2822–2828.
- (32) Gouda, L.; Rietwyk, K. J.; Hu, J.; Kama, A.; Ginsburg, A.; Priel, M.; Keller, D. A.; Tirosh, S.; Gottesman, R.; Zaban, A. High Resolution Study of TiO₂ Contact Layer Thickness on the Performance of Over 800 Perovskite Solar Cells. *ACS Energy Lett.* **2017**, *2*, 2356–2361.
- (33) Liu, X.; Wang, F.; Wang, Q. Nanostructure-Based WO₃ Photoanodes for Photoelectrochemical Water Splitting. *Phys. Chem. Chem. Phys.* **2012**, *14* (22), 7894–7911.
- (34) Huang, Z. F.; Song, J.; Pan, L.; Zhang, X.; Wang, L.; Zou, J. J. Tungsten Oxides for Photocatalysis, Electrochemistry, and Phototherapy. *Adv. Mater.* **2015**, *27* (36), 5309–5327.
- (35) Meyer, J.; Hamwi, S.; Kröger, M.; Kowalsky, W.; Riedl, T.; Kahn, A. Transition Metal Oxides for Organic Electronics: Energetics, Device Physics and Applications. *Adv. Mater.* **2012**, *24* (40), 5408–5427.
- (36) Cho, I. S.; Kwak, C. H.; Kim, D. W.; Lee, S.; Hong, K. S. Photophysical, Photoelectrochemical, and Photocatalytic Properties of Novel SnWO₄ Oxide Semiconductors with Narrow Band Gaps. *J. Phys. Chem. C* **2009**, *113* (24), 10647–10653.

- (37) Kölbach, M.; Jordão Pereira, I.; Harbauer, K.; Plate, P.; Höflich, K.; Berglund, S. P.; Friedrich, D.; van de Krol, R.; Abdi, F. F. Revealing the Performance Limiting Factors in α -SnWO₄ Photoanodes for Solar Water Splitting. *Chem. Mater.* **2018**, *30*, 8322–8331.
- (38) Kölbach, M.; Hempel, H.; Harbauer, K.; Schleuning, M.; Petsiuk, A.; Höflich, K.; Deinhart, V.; Friedrich, D.; Eichberger, R.; Abdi, F. F.; et al. Grain Boundaries Limit the Charge Carrier Transport in Pulsed Laser Deposited α -SnWO₄ Thin Film Photoabsorbers. *ACS Appl. Energy Mater.* **2020**, *3* (5), 4320–4330.
- (39) Schnell, P.; Kölbach, M.; Schleuning, M.; Obata, K.; Irani, R.; Ahmet, I. Y.; Harb, M.; Starr, D. E.; Van de Krol, R.; Abdi, F. F. Interfacial SnO₂ Formation Limits the Photovoltage in α -SnWO₄/NiO_x Photoanodes Prepared by Pulsed Laser Deposition. *Adv. Energy Mater.* **2021**, *11*, 2003183.
- (40) Harb, M.; Cavallo, L.; Basset, J. M. Remarkable Influence of α -SnWO₄ Exposed Facets on Their Photocatalytic Performance for H₂ and O₂ Evolution Reactions. *J. Phys. Chem. C* **2020**, *124* (34), 18684–18689.
- (41) Azofra, L. M.; Cavallo, L.; Basset, J. M.; Harb, M. Need for Rationally Designed SnWO₄ Photo(Electro)Catalysts to Overcome the Performance Limitations for O₂ and H₂ Evolution Reactions. *J. Phys. Chem. C* **2021**, *125* (16), 8488–8496.
- (42) Pignolet, A.; Rao, G. M.; Krupanidhi, S. B. Rapid Thermal Processed Thin Films of Reactively Sputtered Ta₂O₅. *Thin Solid Films* **1995**, *258* (1–2), 230–235.
- (43) Ren, W.; Yang, G. D.; Feng, A. L.; Miao, R. X.; Xia, J. B.; Wang, Y. G. Annealing Effects on the Optical and Electrochemical Properties of Tantalum Pentoxide Films. *J. Adv. Ceram.* **2021**, *10* (4), 704–713.
- (44) Chaneliere, C.; Autran, J. L.; Devine, R. A. B.; Balland, B. Tantalum Pentoxide (Ta₂O₅) Thin Films for Advanced Dielectric Applications. *Mater. Sci. Eng. R Reports* **1998**, *22* (6), 269–322.
- (45) Garg, S. P.; Krishnamurthy, N.; Awasthi, A.; Venkatraman, M. The O-Ta (Oxygen-Tantalum) System. *J. Phase Equilibria* **1996**, *17* (1), 63–77.
- (46) Chun, W. J.; Ishikawa, A.; Fujisawa, H.; Takata, T.; Kondo, J. N.; Hara, M.; Kawai, M.; Matsumoto, Y.; Domen, K. Conduction and Valence Band Positions of Ta₂O₅, TaO_n, and Ta₃N₅ by UPS and Electrochemical Methods. *J. Phys. Chem. B* **2003**, *107* (8), 1798–1803.
- (47) *NIST X-Ray Photoelectron Spectroscopy Database, Version 4.1 (National Institute of Standards and Technology, Gaithersburg, 2012); [Http://Srdata.Nist.Gov/Xps/](http://Srdata.Nist.Gov/Xps/) (accessed in September 2021).*
- (48) Ho, S. F.; Contarini, S.; Rabalais, J. W. Ion-Beam-Induced Chemical Changes in the Oxyanions (MO_{yn}-) and Oxides (MO_x) Where M = Cr, Mo, W, V, Nb, and Ta. *J. Phys. Chem.* **1987**, *91* (18), 4779–4788.
- (49) Kim, J. K.; Chai, S. U.; Y Cho; Cai, L.; Kim, S. J.; Park, S.; Park, J. H.; Zheng, X. Ultrafast Flame Annealing of TiO₂ Paste for Fabricating Dye-Sensitized and Perovskite Solar Cells with Enhanced Efficiency. *Small* **2017**, *13* (42), 1702260.
- (50) Roozeboom, F.; Parekh, N. Rapid Thermal Processing Systems: A Review with Emphasis on Temperature Control. *J. Vac. Sci. Technol. B Microelectron. Nanom. Struct.* **1990**, *8* (6), 1249.
- (51) OPTICS: THE WEBSITE (accessed in July 2021).

<https://www.opticsthewebsite.com/OpticsCalculators>.

- (52) Ojanen, M.; Kärhä, P.; Ikonen, E. Spectral Irradiance Model for Tungsten Halogen Lamps in 340-850nm Wavelength Range. *Appl. Opt.* **2010**, *49* (5), 880–886.
- (53) Wünsch, G. Redox Potentials of Tungsten and Its Alloying Partners—Fundamentals of Tungsten Determination by Redox Titration. *Talanta* **1980**, *27*, 649–654.
- (54) Darmawi, S.; Burkhardt, S.; Leichtweiss, T.; Weber, D. A.; Wenzel, S.; Janek, J.; Elm, M. T.; Klar, P. J. Correlation of Electrochromic Properties and Oxidation States in Nanocrystalline Tungsten Trioxide. *Phys. Chem. Chem. Phys.* **2015**, *17* (24), 15903–15911.
- (55) Berger, T.; Monllor-Satoca, D.; Jankulovska, M.; Lana-Villarreal, T.; Gómez, R. The Electrochemistry of Nanostructured Titanium Dioxide Electrodes. *Chemphyschem* **2012**, *13* (12), 2824–2875.
- (56) Bisquert, J. Physical Electrochemistry of Nanostructured Devices. *Phys. Chem. Chem. Phys.* **2008**, *10* (1), 49–72.
- (57) Minohara, M.; Dobashi, Y.; Kikuchi, N.; Samizo, A.; Tsukuda, K.; Nishio, K.; Mibu, K.; Kumigashira, H.; Hase, I.; Yoshida, Y.; et al. Bipolar Semiconducting Properties in α -SnWO₄ Based on the Characteristic Defect Structure. *Inorg. Chem.* **2021**, *60*, 8035–8041.

Shining a Hot Light on Emerging Photoabsorber Materials: The Power of Rapid Radiative Heating in Developing Oxide Thin-film Photoelectrodes

Ronen Gottesman,^{a*} Isabella Peracchi,^{a,b} Jason L. Gerke,^{a,b} Rowshanak Irani,^a Fatwa F. Abdi,^a and Roel van de Krol^{a,b}

^aInstitute for Solar Fuels, Helmholtz-Zentrum Berlin für Materialien und Energie GmbH, Hahn-Meitner-Platz 1, 14109 Berlin, Germany.

^bInstitut für Chemie, Technische Universität Berlin, Straße des 17. Juni 124, 10623 Berlin, Germany.

ronen.gottesman@helmholtz-berlin.de; roel.vandekrol@helmholtz-berlin.de

1. Experimental Section

Films Deposition: all films were deposited using a PLD system (PREVAC, Poland) by ablating with a KrF-Excimer laser (248 nm, LPXPro 210, COHERENT) commercial targets (SnWO₄, 99.99%, METALLIC FLEX, Ta₂O₅, TiO₂ and WO₃, 99.99%, FHR, Ni 99.99%, Alfa Aesar). The target-to-substrate distance was 60 mm, and all substrates were FTO-coated glass (TEC 7, Pilkington), cleaned in a 1 vol % Triton solution (Triton X-100, Sigma-Aldrich), deionized water, and ethanol (Sigma-Aldrich) for 10 min in each solution. Table S1 shows the PLD and RTP conditions for each material.

Table S1. Summary of the PLD and RTP parameters and conditions used in the study.

Target Material	Laser fluence	PLD Substrate temperature	PLD Background pressure	RTP environment (1 atm)	RTP temperature	Dwell time
α -SnWO ₄	2 J/cm ²	Room temperature	1 × 10 ⁻⁴ millibar	Ar	550 °C	1-8 min
Ni	2 J/cm ²	Room temperature	1 × 10 ⁻² millibar	N/A	N/A	N/A
Ta ₂ O ₅	2.5 J/cm ²	500 °C	1 × 10 ⁻⁶ millibar	O ₂ /Ar/N ₂	850 °C	< 5 sec
TiO ₂	2 J/cm ²	500 °C	1 × 10 ⁻⁶ millibar	80:20 mixture of N ₂ :O ₂	850 °C	< 5 sec

WO ₃	2 J/cm ²	500 °C	1 × 10 ⁻⁶ millibar	80:20 mixture of N ₂ :O ₂	850 °C	< 5 sec
-----------------	---------------------	--------	----------------------------------	---	--------	---------

Furnace heating and rapid thermal processing: Conventional furnace heating of the binary oxides was performed at 500 °C in air at a heating rate of 10 °C/min. Rapid thermal processing (RTP) was conducted using a Rapid Thermal Processor (model: AS-One 100, ANNEALSYS). In a typical RTP procedure, a sample is placed on a SiC wafer, used as a susceptor, with an optical pyrometer monitoring the temperature of the SiC. Additionally, the surface temperatures of the samples were monitored by a thermocouple attached to the surface with an indium contact. The susceptor with the sample placed on top is slowly heated to 400 °C (rate = 1 K/sec) and then maintained at that temperature for 5 minutes. Next, the temperature is rapidly increased to the desired process temperature. In the case of SnWO₄, the desired temperature was 550 °C (rate = 10 K/sec), which was maintained for 1 to 8 minutes. In the case of the binary oxides, the RTP was configured to shut off the illumination when the temperature reached 850 °C. At the highest heating rates of 90 K/sec, the maximum temperature overshoots were ~ 30 °C, and the dwell time is defined as the length of time ≥ 850 °C (i.e., ~ 850 – 880 °C). The dwell time at each desired temperature appears in Table S1. In all cases, when illumination shuts off, the temperature decreases below 300 °C after ~ 1 min and reaches room temperature after ~ 10 min.

Characterization: X-ray diffraction (XRD) measurements were performed using a Bruker D8 diffractometer with Cu K α radiation. Measurements were carried out in a grazing incidence geometry (angle of incidence was 2 degrees) with a step size of 0.04 degrees and a step duration of 6 sec. The data were normalized after removing the background without additional data averaging or noise reduction. X-ray photoelectron spectroscopy (XPS) was performed with a SPECS PHOIBOS 100 analyzer at a base pressure of ~10⁻¹⁰ mbar. Monochromatic Al K α radiation (h ν = 1486.74 eV, SPECS FOCUS 500

monochromator) was applied with the pass energy of 30 and 10 eV. The step sizes were chosen to be 0.5 eV for the survey and 0.05 eV for the fine spectra. For fitting the peaks, XPSPEAK software with Voigt profiles and a Shirley background subtraction was applied. The adventitious carbon (C 1s) peak at a binding energy of 284.5 eV was used for the calibration of binding energies.

UV-VIS measurements were performed using a PerkinElmer Lambda 950 spectrophotometer with an integrating sphere. Samples were placed inside the integrating sphere with an offset of $\sim 7.5^\circ$ from the incident light, and the transmittance TR (transmittance T + reflectance R) was measured. SEM imaging was carried out at a Zeiss UltraPlus scanning electron microscope operated at 12.5 kV acceleration voltage. The grain sizes were quantified by using the ImageJ software.

Photoelectrochemical measurements were performed in the three-electrode configuration under the control of a potentiostat (EG&G Princeton Applied Research 273A). The studied films were connected as the working electrode in a custom-designed PEC cell with a calibrated Ag/AgCl reference electrode (XR300, Radiometer Analytical, $E_{\text{Ag/AgCl}} = 0.199$ V vs. normal hydrogen electrode, NHE), and a platinum wire as the counter electrode. All the measured potentials were converted to the reversible hydrogen electrode (RHE) scale using the Nernst equation. The illuminated area of the sample was 0.28 cm^2 , which is identical to the area exposed to the electrolyte. The electrolyte used to measure the $\alpha\text{-SnWO}_4$ was a 0.5 M potassium phosphate (KPi) buffer solution prepared by adjusting the ratio of KH_2PO_4 (99%, Sigma-Aldrich) and K_2HPO_4 (99%, Sigma-Aldrich) to obtain a pH 7 solution. 0.5 M Na_2SO_3 (99%, Sigma-Aldrich) was added as a hole scavenger. Measurements of the binary oxides were performed in 0.1 M boric acid (H_3BO_3 , 99.5%, Merck) at pH 9. A WACOM super solar simulator (Model WXS-50S-5H, class AAA) was used as the illumination source and calibrated to closely resemble the AM1.5 global spectrum at 100 mW cm^{-2} .

For incident photon-to-current efficiency (IPCE) measurements, a LOT (LSH302) lamp and Acton Research monochromator (SP2150) were used. The incident-photon-to-current conversion efficiency (IPCE) values were calculated as follows:

$$IPCE (\%) = \frac{J_P (mA\ cm^{-2}) * 1240 (V\ nm)}{P (mW\ cm^{-2}) * \lambda (nm)} * 100 \quad (1)$$

Where J_p is the averaged photocurrent density, P is the power density of the incident light, and λ is the wavelength. The power density was calibrated through the electrolyte contained between two quartz windows for front-side illumination and through FTO glass for backside illumination. This means that the reported IPCE values are for the film itself and not for the entire photoanode / PEC cell assembly. Absorbed photon-to-current efficiency (APCE) values were calculated by dividing the IPCE through the absorbance of the measured photoelectrode:

$$APCE (\%) = \frac{IPCE (\%)}{\text{Absorbance}} \quad (2)$$

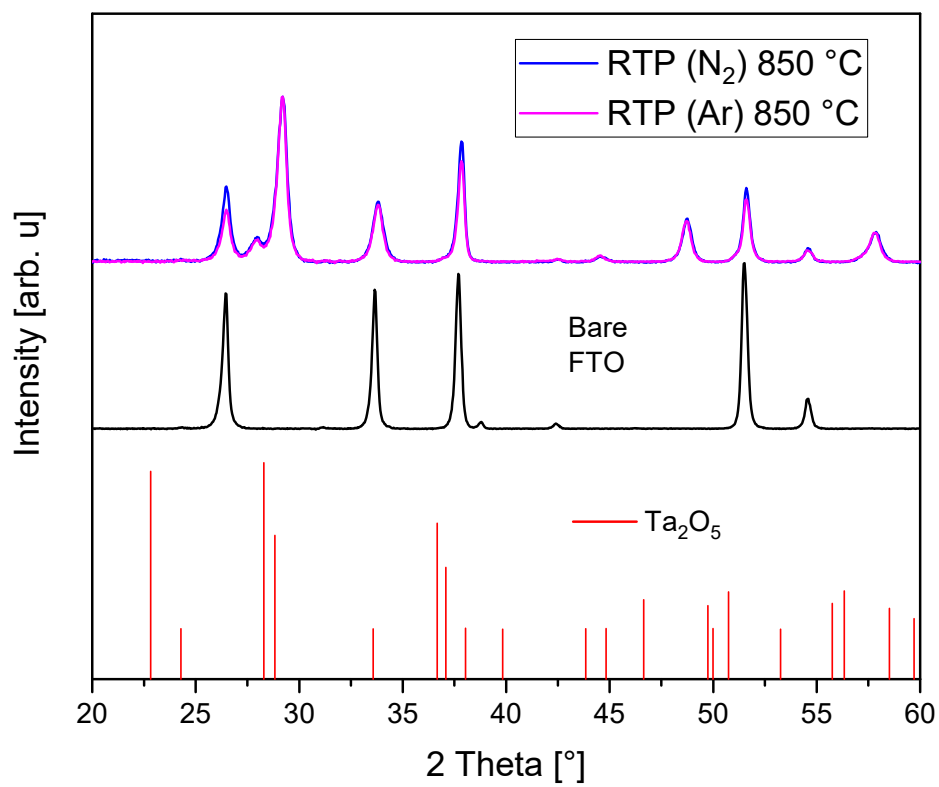


Figure S1. X-ray diffractograms of a bare FTO substrate, Ta_xO_y on FTO: after RTP at 850 °C in Ar and N₂ at a rate of ~ 90 °C/sec. Ta₂O₅ PDF: 01-082-9637.

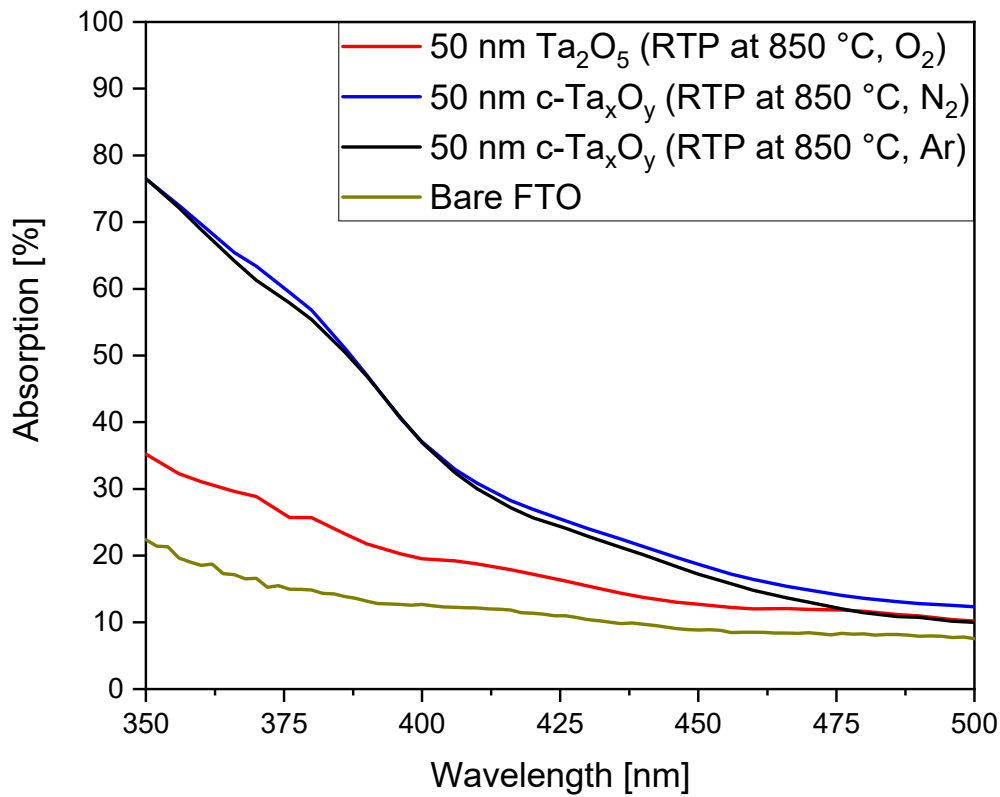


Figure S2. The absorption spectra of RTP-treated Ta_xO_y films under O_2 , Ar, and N_2 . The spectrum of bare FTO is shown as a reference.

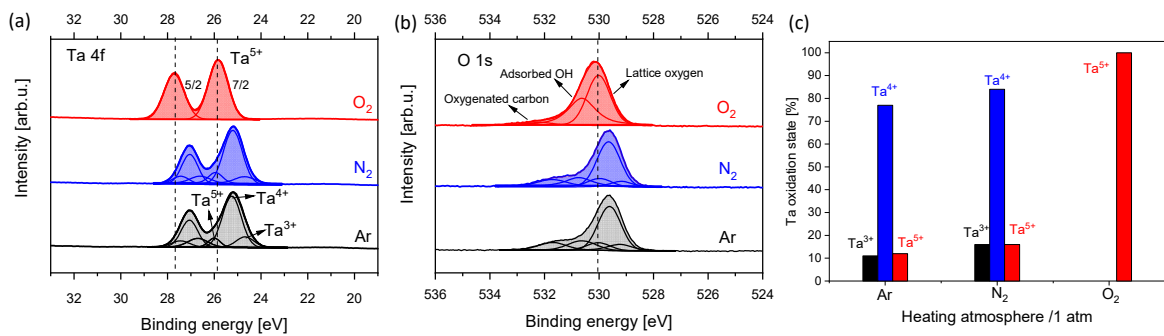


Figure S3. XPS spectra of a) Ta 4f, and b) O 1s core levels from top to bottom: RTP-treated Ta_xO_y films under O_2 , Ar, and N_2 . Heating under O_2 results with Ta_2O_5 , whereas in the films heated under N_2 and Ar multiple, lower oxidation states exist. C) Oxidation states quantities of Ta for each heating atmosphere.

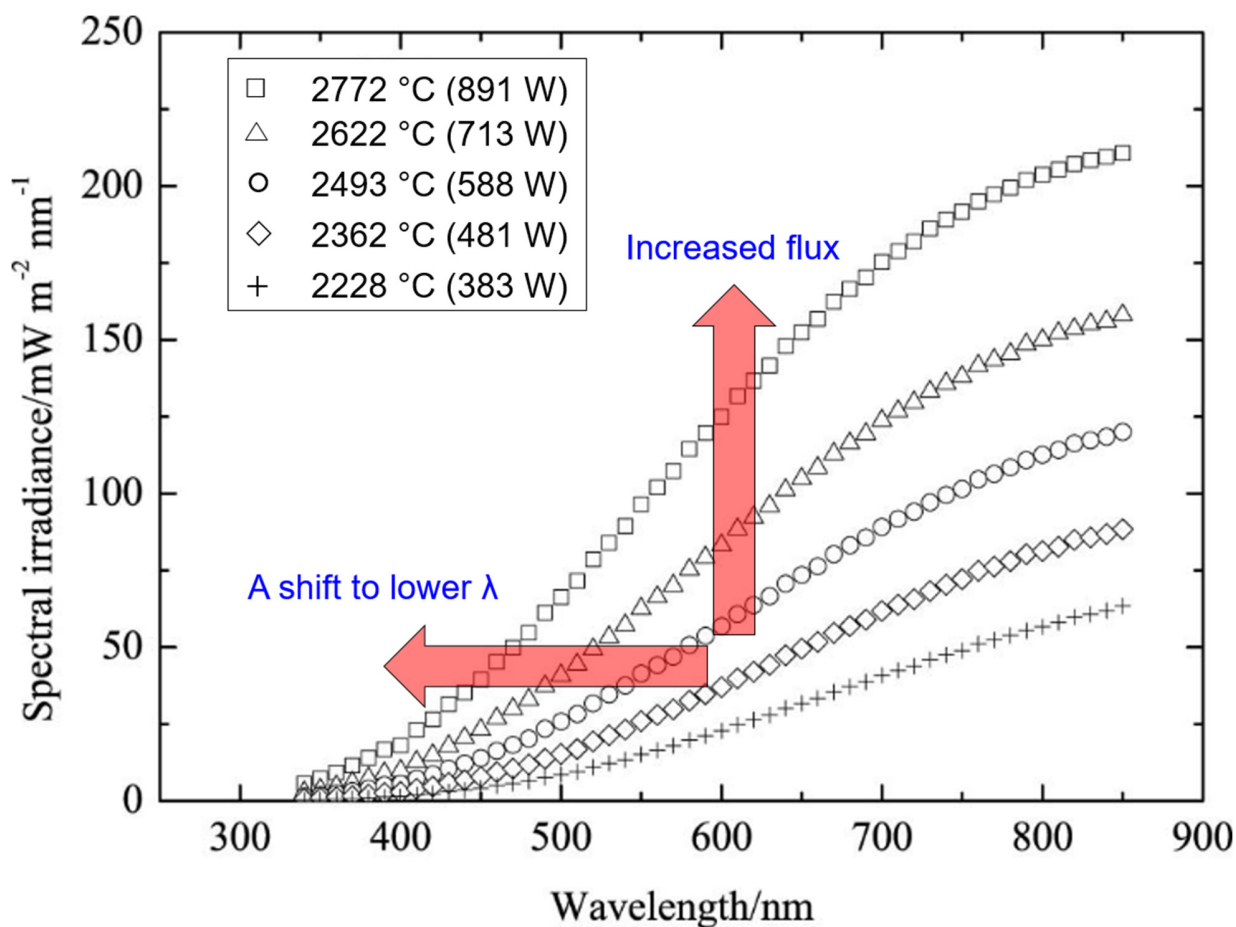


Figure S4. Measured spectral irradiances of a tungsten halogen lamp at different powers/temperatures. Modified from ref ¹.

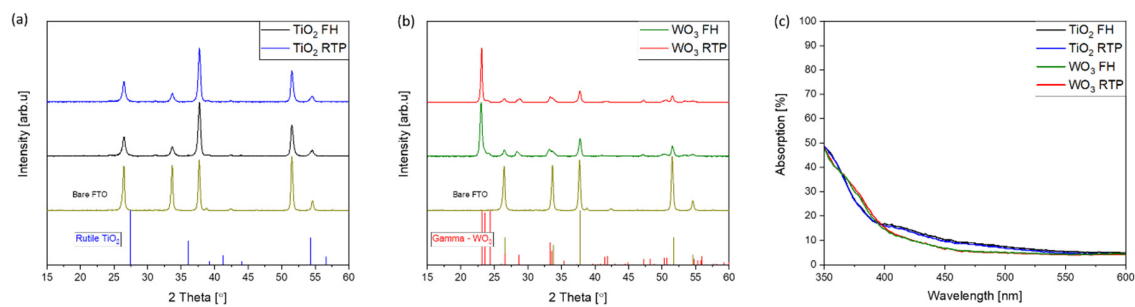


Figure S5. a, b) X-ray diffractograms of the 30 nm TiO₂ and WO₃ photoelectrodes (and bare FTO as a reference), heated by RTP at 850 °C (15°C/sec, an 80:20 mixture of N₂:O₂) and FH at 500 °C (in air). c) The absorption spectra of all four photoelectrodes.

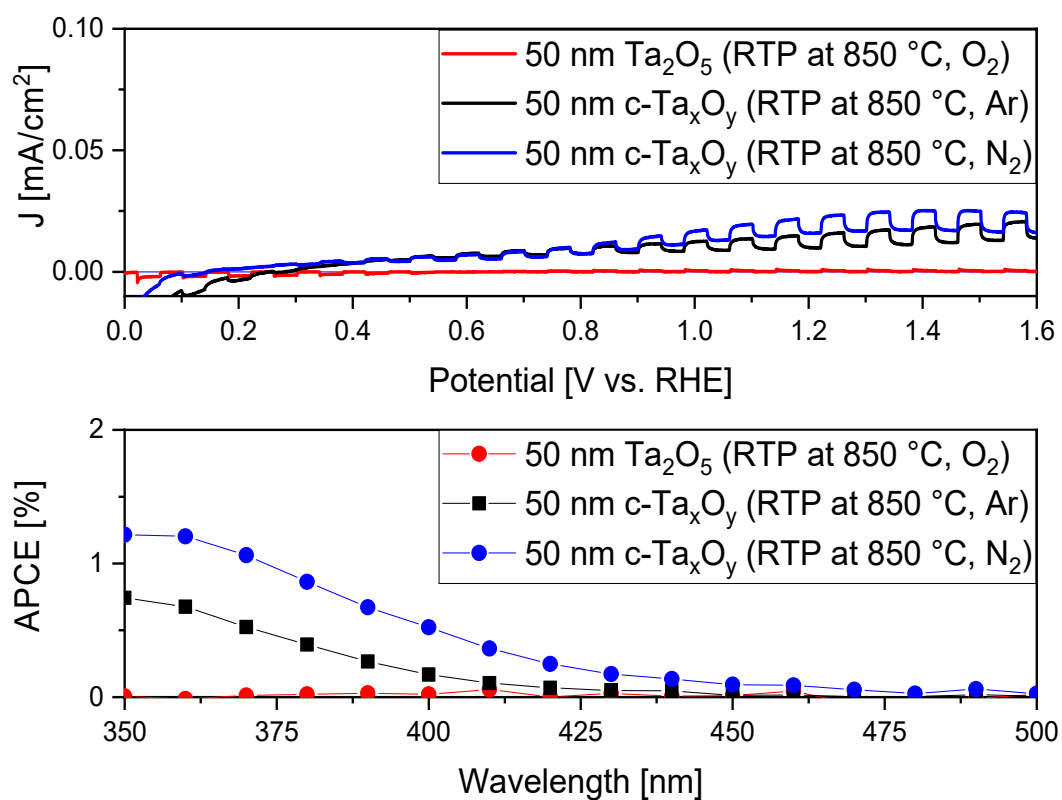


Figure S6. Chopped LSV scans and APCE spectra of RTP-treated Ta_xO_y photoelectrodes under O₂, Ar, and N₂. The measurements were performed in 0.1 M boric acid (pH 9) under front-side illumination. These low photocurrents can result from one or more of the following factors: i) low specific surface area, ii) high bandgap energy that decreases the available light-harvesting range, iii) un-optimized films thickness, and iv) poor charge transport, which can lead to high recombination rates. A complete understanding of the carrier dynamics of these photoelectrodes and their structure cannot be resolved here is beyond the scope of this study.

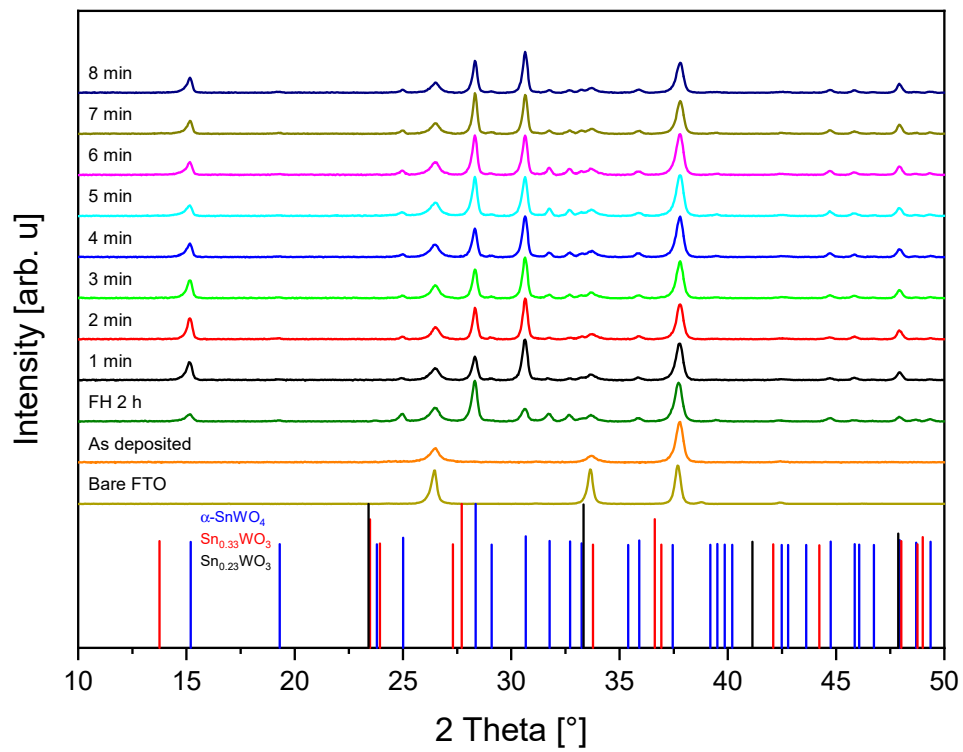


Figure S7. X-ray diffractograms of 1 – 8 min RTP-treated and FH 2 h-treated 100 nm α -SnWO₄ photoelectrodes, shown on a shared baseline, with bare FTO as a reference.

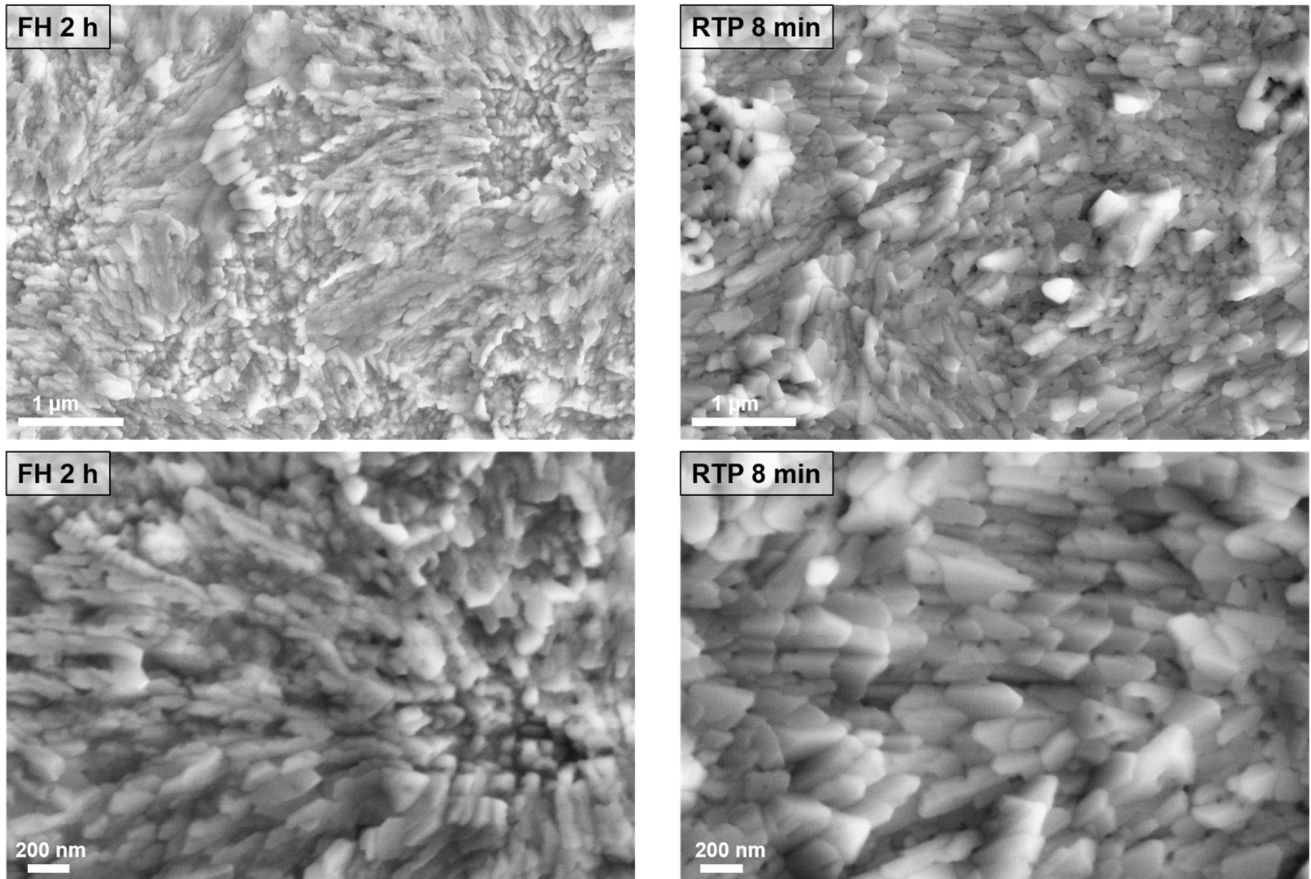


Figure S8. Top-view SEM images of α -SnWO₄ photoelectrodes after heating by FH for 2 h at 550 °C in Ar, and by RTP for 8 min at 550 °C in Ar. The average grain sizes (length and width) – FH: 233 ± 89 and 106 ± 36 nm, and RTP: 466 ± 90 and 172 ± 43 nm.

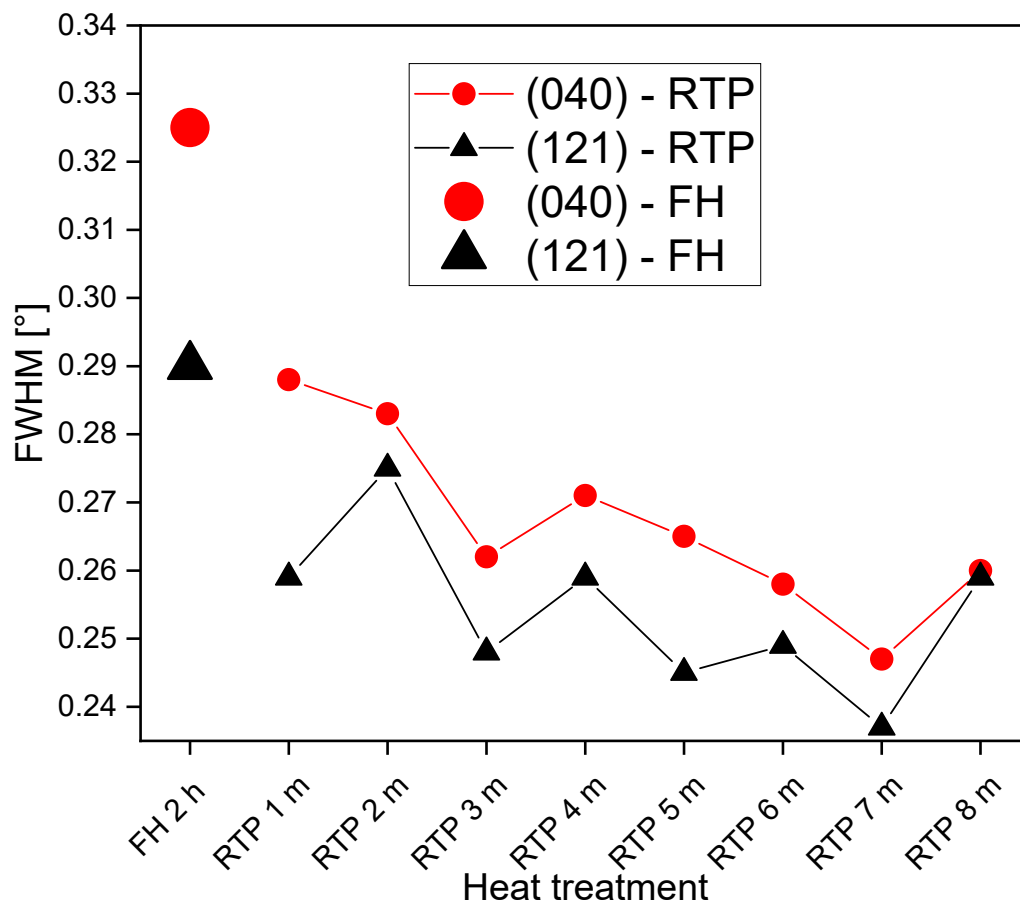


Figure S9. The FWHM of the (040) and (121) peaks plotted against the type and duration of heating treatment.

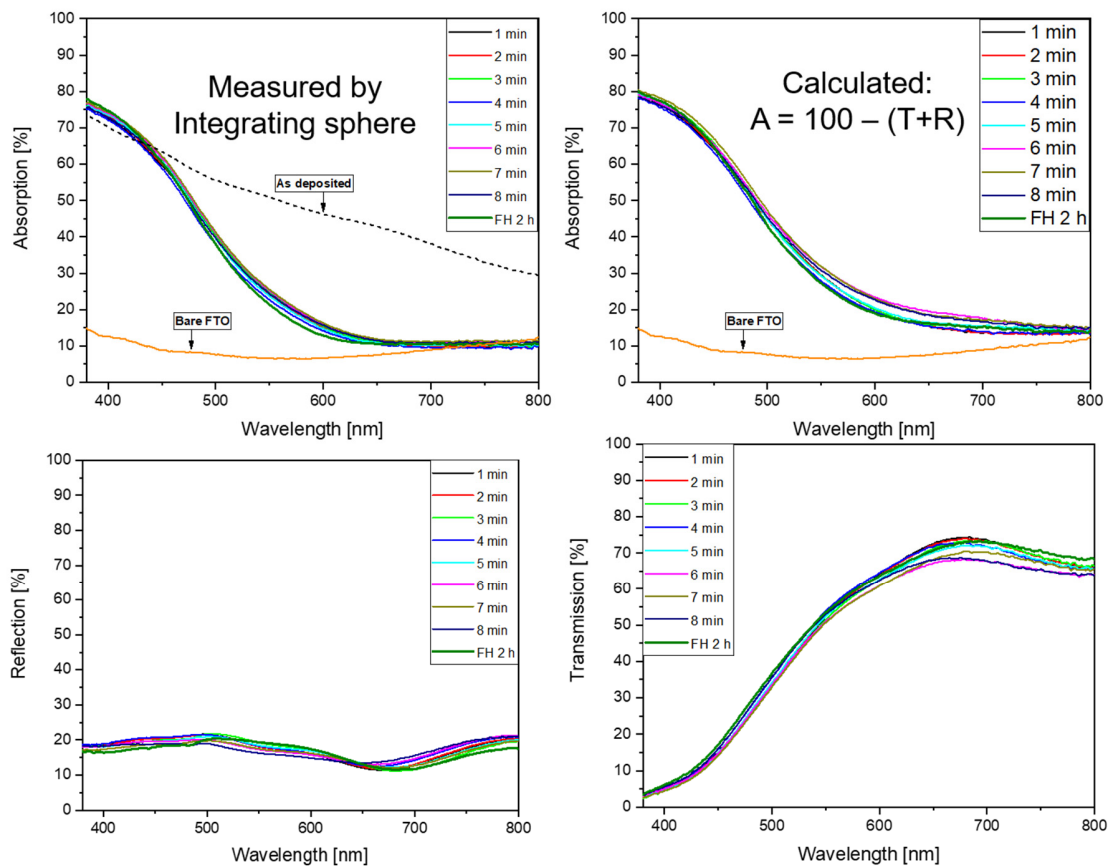


Figure S10. UV-VIS measurements of α -SnWO₄ films heated by both methods. Top: absorption plots, which were obtained by either measuring directly using an integrating sphere or by calculation by using the separately measured reflection and transmittance values that appear in the bottom plots.

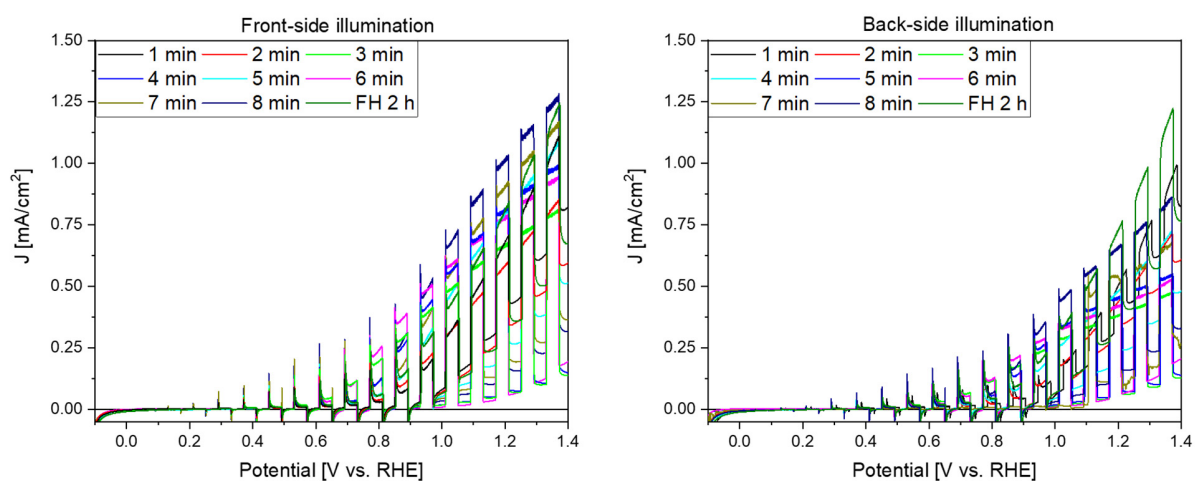


Figure S11. Chopped linear sweep voltammetry scans of the 1 – 8 min RTP-treated and FH 2 h-treated 100 nm α -SnWO₄ photoelectrodes.

References:

- (1) Ojanen, M.; Kärhä, P.; Ikonen, E. Spectral Irradiance Model for Tungsten Halogen Lamps in 340-850nm Wavelength Range. *Appl. Opt.* **2010**, *49* (5), 880–886.